International Journal of Current Science Research and Review
ISSN: 2581-8341
Volume 09 Issue 07 July 2026
DOI: 10.47191/ijcsrr/V9-i7-59, Impact Factor: 8.048
IJCSRR @ 2026
www.ijcsrr.org

Selective Iron Suppression through Sulfation, Oxidative Calcination, and pH-Controlled Atmospheric Leaching of a Ferruginous Oxidized Copper Ore

Antonio Clareti Pereira, PhD
PhD in Chemical Engineering
University of São Paulo (USP), Belo Horizonte, Minas Gerais, Brazil
ORCID: https://orcid.org/0000-0001-8115-4279

ABSTRACT: Iron-rich oxidized copper ores are challenging to treat by atmospheric leaching because iron oxides and oxyhydroxides may consume acid and increase impurity loading in the pregnant leach solution. This study evaluated a three-stage route comprising sulfuric-acid sulfation, oxidative calcination, and pH-controlled atmospheric leaching, with the primary objective of minimizing net Fe transfer rather than maximizing Cu extraction. Six distinct operating conditions were investigated using a ferruginous oxidized copper ore from northern Bahia, Brazil, containing 19.6 wt.% Fe, 5.37 wt.% Al, 1.47 wt.% Mg, 0.524 wt.% Mn, and 1.05 wt.% Cu. Commercial sulfuric-acid solution additions during sulfation ranged from 9.75 to 99.69 kg solution/t dry ore. The sulfated products were calcined through staged temperatures from approximately 250 to 700 °C over 6 h and subsequently leached at approximately 90 °C for 180 min, with final solution pH values of 2.33–2.77. Reconciled Fe transfer remained between 0.026% and 0.340%, corresponding to Fe suppression of 99.66–99.97%. By contrast, Mg, Mn, and Al transfers ranged from 6.39% to 29.78%, 38.14% to 59.98%, and 6.95% to 16.28%, respectively, confirming that Fe suppression did not result from a general inhibition of mineral dissolution. The measured Fe transfers corresponded to calculated stoichiometric acid equivalents of only 0.13–1.76 kg H_2SO_4/t ore, compared with an upper-bound requirement of 516.34 kg H_2SO_4/t ore for complete conversion and dissolution of feed Fe as Fe(III) sulfate. The response is consistent with initial formation of ferric sulfate, basic ferric sulfate, or related Fe-bearing sulfate intermediates, followed by thermal destabilization to poorly soluble Fe(III)-oxide-bearing phases and release of sulfur oxides. Released SO_3 may have promoted sulfate redistribution to neighboring reactive metal–oxygen sites, while controlled-pH leaching was consistent with an additional aqueous Fe-rejection barrier through limited Fe-oxide attack and Fe(III) hydrolysis or reprecipitation. Mg behaved as a persistent sulfate sink, Mn showed redox-sensitive transfer, and Al exhibited intermediate behavior. The route therefore selectively decoupled the large Fe inventory from the final aqueous products. Direct-leaching controls and stage-resolved mineralogical, sulfur-speciation, and off-gas analyses are required to quantify actual acid savings and confirm the proposed mechanism.

KEYWORDS: Selective iron suppression, ferruginous oxidized copper ore, sulfuric-acid sulfation, oxidative calcination, atmospheric leaching, pH-controlled leaching

Highlights

- Sulfation, oxidative calcination to approximately 700 °C, and pH-controlled leaching limited reconciled Fe transfer to 0.026–0.340%.
- The corresponding Fe suppression of 99.66–99.97% reduced the measured ferric-iron acid liability to only 0.13–1.76 kg H_2SO_4/t ore.
- Ferric-sulfate formation and decomposition provide a plausible internal sulfate-redistribution pathway while regenerating poorly soluble Fe_2O_3.
- Mg and Mn were not comparably suppressed, confirming that low Fe transfer did not result from a general inhibition of all gangue dissolution.
- The route should be assessed primarily by iron rejection and avoided Fe-related acid demand, not by maximum copper extraction.

International Journal of Current Science Research and Review
ISSN: 2581-8341
Volume 09 Issue 07 July 2026
DOI: 10.47191/ijcsrr/V9-i7-59, Impact Factor: 8.048
IJCSRR @ 2026
www.ijcsrr.org

Graphical abstract

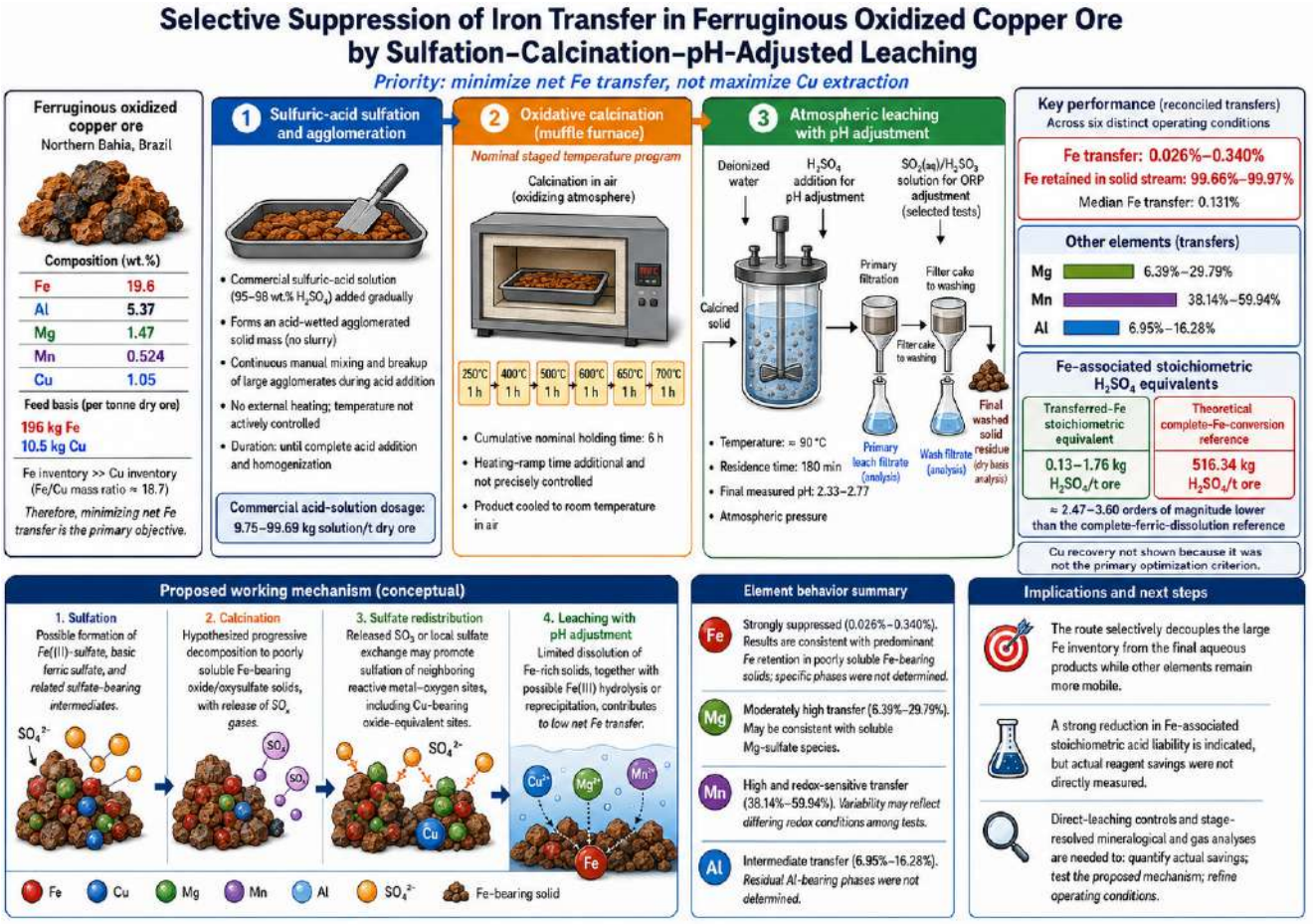

1. INTRODUCTION

1.1. Iron as the principal acid-liability driver in atmospheric leaching

Atmospheric sulfuric acid leaching is attractive for oxidized ores because it operates at moderate temperatures and pressures, but its selectivity is often governed by the gangue rather than the target metal. Carbonates, reactive silicates, clays, secondary precipitates, and iron-bearing phases can consume acid, retard transport, increase solution viscosity, and complicate downstream purification. These effects have been documented in copper and lateritic systems, where mineralogy, particle size, residence time, and gangue reactivity can dominate the apparent metallurgical response (Thomas, 2021; Toro et al., 2021; Dong et al., 2023; Kutluata & Obut, 2026; Tang et al., 2023; Vehmaanperä et al., 2021; Yeskibayeva et al., 2024; Pereira, 2026a, 2026b).

Iron is especially consequential because ferruginous ores may contain one to two orders of magnitude more Fe than the valuable metal. If Fe enters solution, it consumes acid during dissolution and subsequently demands neutralization or precipitation, generating additional residue and potentially entraining valuable metals. Studies of iron precipitation from laterite liquors, goethite and hematite formation, jarosite chemistry, and basic ferric sulfate show that Fe control is not a single reaction but a coupled problem of oxidation state, hydrolysis, sulfate activity, temperature, seeding, and precipitation kinetics (Buriti et al., 2024, 2025; Cruells & Roca, 2022; da Silva et al., 2022; Das & Li, 2023; Deng et al., 2020; Febriana et al., 2026; Ventruti et al., 2020). Scaling and solid deposition under high-acid laterite conditions further demonstrate that uncontrolled Fe chemistry can affect both solution quality and equipment performance (Dickson et al., 2026), while alternative atmospheric routes seek to retain Fe in a manageable solid form before or during leaching (Xiao et al., 2026).

The feed studied here contained 19.6 wt.% Fe and 1.05 wt.% Cu, equivalent to approximately 196 kg Fe and 10.5 kg Cu per tonne of dry ore. This Fe/Cu mass ratio of approximately 18.7 makes Fe suppression a first-order process objective. The relevant

International Journal of Current Science Research and Review
ISSN: 2581-8341
Volume 09 Issue 07 July 2026
DOI: 10.47191/ijcsrr/V9-i7-59, Impact Factor: 8.048
IJCSRR @ 2026
www.ijcsrr.org

question is therefore not whether the highest possible fraction of Cu can be transferred, but whether accessible Cu-bearing sites can be activated while Fe remains in a refractory or readily reprecipitated form.

1.2. Sulfation and roasting as selective phase-transformation tools

Sulfation followed by roasting, calcination, water leaching, or acid leaching has been investigated across a wide range of feed materials, including Ti-bearing slags, bauxite residues, limonitic and saprolitic laterites, rare-earth ores, serpentine-rich ores, refractory oxidized ores, and industrial residues. Collectively, these studies show that selectivity arises from differences in sulfate formation, thermal stability, decomposition kinetics, and final sulfate solubility rather than from a universal sulfate-roasting mechanism (Bian et al., 2020; Dong et al., 2022; Falah et al., 2026; Gontijo et al., 2023; Maluleke et al., 2023; Teixeira, 2020; Tauakelov et al., 2025).

Recent laterite investigations have emphasized the need to couple mineralogy with thermal and aqueous operating windows. Sulfation-roasting-leaching responses depend on serpentine abundance, MgO and SiO_2 contents, alkali salts, pre-roasting, roasting temperature, sulfate dose, and post-roast leaching conditions (Hariyanto et al., 2023a, 2023b, 2024; Mamyrbayeva et al., 2025; Osali et al., 2026; Ribeiro et al., 2020, 2021, 2022; Yang et al., 2022; Zhao et al., 2024, 2025b). Microwave and alternative thermal activation studies likewise show that the heating mode and mineral decomposition pathway can materially alter leachability (Muhammad et al., 2025).

A related body of work has treated sulfation roasting as an integrated chemical loop in which sulfur oxides are generated, retained, transferred, or recovered. Enhanced SO_3 recovery, oxidative decomposition roasting, and process integration have been proposed for laterites and ferronickel systems, underscoring that the fate of sulfur during heating is central to both selectivity and reagent efficiency (Qin et al., 2026; Zhao et al., 2025a). The present study applies this phase-transformation concept specifically to the rejection of Fe from a ferruginous oxidized copper ore.

1.3. Ferric sulfate decomposition, sulfate redistribution, and furnace atmosphere

Low-temperature sulfation of iron oxides and hydroxides can yield ferric sulfate or basic ferric sulfate, depending on acid activity, water content, and mineral reactivity (Gontijo et al., 2020; Ventruti et al., 2020). During heating, Fe-bearing sulfate phases undergo dehydration, changes in oxidation state, oxysulfate formation, and decomposition into iron oxides. High-temperature characterization of melanterite and kinetic studies of $FeSO_4$ decomposition indicate that Fe(II)-sulfate pathways are complex and atmosphere-sensitive (Lacalamita et al., 2021; Rego et al., 2024). Ferrous-sulfate transformations during hematite precipitation and solid-state oxidation studies further show that oxygen availability controls the pathway by which Fe(II) phases evolve toward Fe(III) oxides (Deng et al., 2020; Klyushnikov et al., 2021, 2023).

Iron sulfate can also behave as a sulfating agent. Experimental roasting of copper-slag tailings with iron sulfates and thermodynamic studies of Fe(III)-sulfate-assisted upgrading demonstrate that ferric sulfate may redistribute sulfate to other reactive phases while Fe is converted to an oxide (Grudinsky et al., 2021; Souza et al., 2022). Hematitization baking has similarly been used to improve Fe selectivity during base-metal leaching (Kart et al., 2021). Thermodynamic modeling of multimetal sulfate roasting and experimental roasting studies confirm that the relative stability of Fe, Cu, Co, Ni, and gangue sulfates is highly dependent on temperature and gas composition (Sun et al., 2026; Urtnasan et al., 2024; Zhang et al., 2026).

Copper-bearing feeds provide additional evidence that SO_2–O_2 or sulfate-mediated roasting can convert Cu into a water- or acid-soluble sulfate while Fe remains in less-soluble oxide forms. Such behavior has been reported for copper-bearing materials, low-nickel and low-grade nickel mattes, copper slags, and waste-on-waste roasting systems (Gayratov et al., 2026; Sun et al., 2020; Wan et al., 2020, 2021; Xiao et al., 2021). Thermal decomposition and leaching studies of copper-containing intermediates also show that the final Cu phase depends on the thermal decomposition path and the availability of sulfur-bearing species (Sari et al., 2026). These studies support, but do not directly prove for the present ore, a local sulfate-transfer mechanism involving ferric sulfate or SO_3 released during its decomposition.

1.4. Why Mg, Mn, and Al require separate interpretation

Selective Fe suppression does not imply suppression of all gangue metals. Mg-bearing silicates can react extensively with sulfuric acid, and $MgSO_4$ may remain stable over temperature ranges where ferric sulfate decomposes. Research on serpentine, peridotite, laterite residues, and magnesium-salt production illustrates the high sulfate affinity and persistence of Mg in acid-treated systems (Peng et al., 2021; Reddy et al., 2020; Taheri & Larachi, 2025; Wanderley et al., 2020). The influence of MgO on sulfation-

International Journal of Current Science Research and Review
ISSN: 2581-8341
Volume 09 Issue 07 July 2026
DOI: 10.47191/ijcsrr/V9-i7-59, Impact Factor: 8.048
IJCSRR @ 2026
www.ijcsrr.org

roasting selectivity and the interaction of serpentinite with dilute sulfuric acid reinforce the need to treat Mg as a separate sulfate sink (Hariyanto et al., 2024; Yeskibayeva et al., 2024).

Al-bearing phases occupy an intermediate position. Thermal activation of alunite, ammonium-sulfate roasting of bauxite, and kinetic studies of K-alum and aluminum sulfate indicate that Al sulfate can form, dehydrate, decompose, and redistribute sulfur over a broad temperature range (Chen et al., 2026; Rego et al., 2021; Xu et al., 2022; Zheng et al., 2020). Silicate decomposition during sulfuric-acid treatment is also governed by mineral structure, diffusion, and the formation of reaction rims (Thibault et al., 2026). Consequently, Al may act as a persistent acid consumer, a temporary sulfate carrier, or a refractory aluminosilicate component, depending on its host phase and the exact furnace history.

Mn is different again because its aqueous transfer is strongly redox-sensitive. In the present tests, sulfurous acid was added to some leaches, so Mn dissolution cannot be interpreted solely by sulfate thermal stability. This contrast among Fe, Mg, Mn, and Al is important: a route that specifically suppresses Fe can still produce substantial Mg, Mn, and Al transfer.

1.5. Objective and working hypotheses

The objective of this study was to quantify and interpret the effectiveness of sulfuric-acid sulfation followed by oxidative calcination and pH-controlled atmospheric leaching in suppressing net Fe transfer from a ferruginous oxidized copper ore. Copper transfer was used only as a process-response tracer. The work tested four linked hypotheses: (i) accessible Fe oxides and oxyhydroxides can initially react with H_2SO_4 to form ferric sulfate or related Fe(III) sulfate phases; (ii) oxidative calcination decomposes these phases, regenerates poorly soluble Fe_2O_3, and releases sulfur oxides; (iii) released SO_3 or direct solid-state exchange can sulfate neighboring reactive Cu-, Mg-, or Al-bearing sites; and (iv) controlled-pH leaching provides a second Fe barrier by limiting renewed Fe-oxide dissolution and promoting hydrolysis of any Fe(III) released. The study further evaluates why Mg and Mn were not suppressed and why Al displayed intermediate behavior.

2. MATERIALS AND METHODS

2.1. Ore provenance and test-feed preparation

The material was supplied to the research project as oxidized copper ore from northern Bahia, Brazil. The process feed was prepared as a homogenized blend of oxidized-ore subsamples. Individual sample identifiers are omitted because the objective is process selectivity rather than deposit-scale mineralogical variability. The mineralogical values reported below are averages for the oxidized-ore group.

2.2. Chemical and modal characterization

The chemical composition of the homogenized process feed is presented in Table 1. Reporting the full feed composition before the operating matrix is essential because the magnitude of the Fe inventory defines the acid-liability problem addressed by the route.

Table 1. Chemical composition of the ferruginous oxidized copper-ore feed.

Constituent	Concentration
Cu	1.05 wt.%
Fe	19.6 wt.%
Al	5.37 wt.%
Mg	1.47 wt.%
Mn	0.524 wt.%
Si	21.5 wt.%
Ca	0.069 wt.%
Zn	44.28 mg/kg

International Journal of Current Science Research and Review
ISSN: 2581-8341
Volume 09 Issue 07 July 2026
DOI: 10.47191/ijcsrr/V9-i7-59, Impact Factor: 8.048
IJCSRR @ 2026
www.ijcsrr.org

Constituent	Concentration
Co	<0.030 wt.%
Cr	<0.200 wt.%
Ni	<0.178 wt.%
Loss on ignition	6.82 wt.%

Authors' compilation from the original project chemical-assay certificate.

The feed contained approximately 196 kg Fe/t ore, compared with 10.5 kg Cu/t. This difference means that dissolving only a small fraction of Fe can consume as much acid as a much larger relative transfer of Cu. Al and Mg were also present at substantial levels, while Mn occurred at a lower bulk concentration but in potentially reactive oxide phases.

Table 2 presents the average modal mineralogy of the oxidized-ore group. Only average values are shown, as requested, to provide a representative mineralogical basis without linking the six process tests to individual drill-core identifiers.

Table 2. Average modal mineralogy of the oxidized copper ore.

Mineral phase	Average modal abundance (wt.%)
Quartz	14.07
Chlorite	8.91
Biotite	31.70
Garnet	9.70
Kaolinite	2.04
Mn oxides	1.53
Fe oxyhydroxides	28.27
Other minerals	3.80

Authors' calculation from the modal-mineralogy dataset supplied with the project; rounded values total approximately 100%.

Within the characterized oxidized-ore group, Fe oxyhydroxides averaged 28.27 wt.%, whereas biotite and chlorite together averaged 40.61 wt.%. These values provide a representative mineralogical context but should not be interpreted as a direct modal analysis of the exact process-test blend.

Biotite and Fe oxyhydroxides were the dominant phases. Fe oxyhydroxides constitute the principal ferruginous reservoir, while biotite and chlorite are major hosts of Mg and Al and may contain structurally bound or finely dispersed Cu. The low average abundance of Mn oxides does not imply low reactivity, particularly under reducing, acidic conditions. The modal assemblage therefore predicts distinct Fe, Mg, Mn, and Al responses rather than uniform gangue behavior.

2.3. Sulfation and staged oxidative calcination

Six tests were conducted using approximately 200 g of dry ore per test. Commercial sulfuric acid was mixed with the ore at nominal additions ranging from 9.75 to 99.69 kg H_2SO_4/t dry ore. The treated material was heated in a muffle furnace at staged temperatures from approximately 250 to 700 °C over a total period of about 6 h. Activation-stage mass loss increased from 5.64 to 9.62% as acid addition increased.

The original furnace records did not include continuous measurements of O_2, SO_2, or SO_3. The treatment is therefore described as nominally oxidative muffle-furnace calcination. The mechanistic interpretation assumes that oxygen was available to favor Fe(III)-oxide formation; controlled gas-flow experiments are required to validate this assumption.

International Journal of Current Science Research and Review
ISSN: 2581-8341
Volume 09 Issue 07 July 2026
DOI: 10.47191/ijcsrr/V9-i7-59, Impact Factor: 8.048
IJCSRR @ 2026
www.ijcsrr.org

2.4. pH-controlled atmospheric leaching

After calcination, approximately 190–199 g of product was leached with approximately 500 g of water at about 90 °C for 180 min. Sulfuric acid was added during leaching to adjust pH. Sulfurous acid was used in some tests to adjust the oxidation–reduction potential (ORP), so Mn behavior is interpreted as a combined thermal and redox response rather than as a function of sulfation dosage alone. Final pregnant-leach-solution pH values ranged from 2.33 to 2.77.

The complete experimental and conceptual sequence is shown schematically in Figure 1. The figure should distinguish the thermal Fe-rejection barrier from the aqueous pH-control barrier.

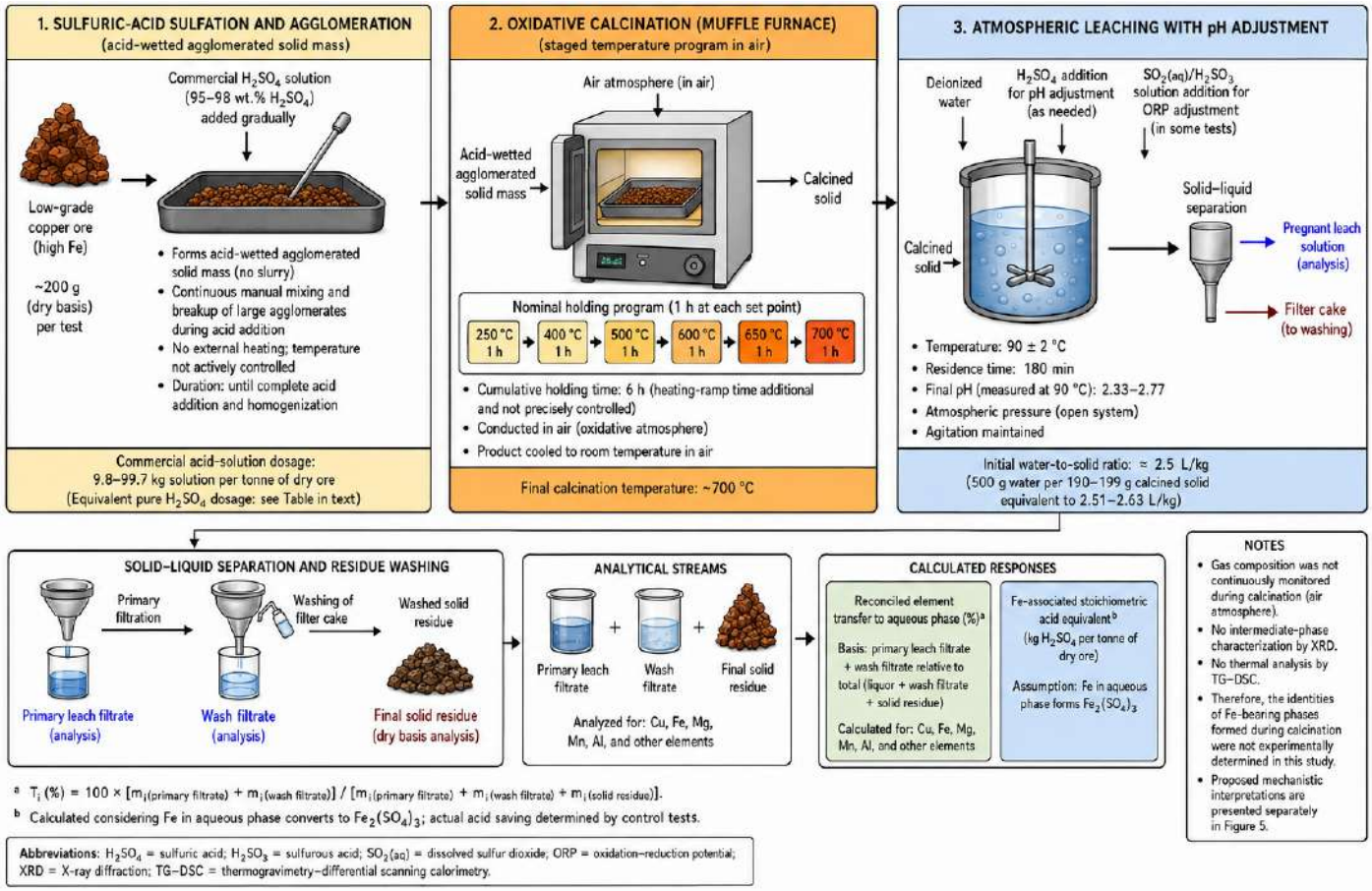

Figure 1. Experimental and conceptual flowsheet for sulfuric-acid sulfation, oxidative calcination, and pH-controlled atmospheric leaching, showing the thermal and aqueous barriers that suppress net Fe.
Source: Authors' elaboration from the original sulfation, calcination, and leaching operating records.

The figure should emphasize that the measured low Fe inventory is an integrated response across the entire route. The current dataset does not isolate the individual contributions of sulfation, calcination, and pH control; dedicated stage-by-stage controls are required to achieve mechanistic separation.

The operating matrix is summarized in Table 3. The table outlines the common thermal and aqueous framework and the variables that varied across the six screening tests.

International Journal of Current Science Research and Review
ISSN: 2581-8341
Volume 09 Issue 07 July 2026
DOI: 10.47191/ijcsrr/V9-i7-59, Impact Factor: 8.048
IJCSRR @ 2026
www.ijcsrr.org

Table 3. Sulfation, calcination, and pH-controlled atmospheric-leaching conditions.

Test	H_2SO_4 in sulfation (kg/t)	Calcination mass loss (%)	Leach T (°C)	Time (min)	Final PLS pH	Final ORP (mV)	H_2SO_3 added (mL)
1	9.75	5.64	90	180	2.67	495	1.03
2	19.80	6.12	90	180	2.70	362	5.15
3	29.94	6.04	90	180	2.35	458	2.06
4	49.99	7.54	90	180	2.33	477	1.03
5	60.05	7.67	89.5–92	180	2.48	445	1.03
6	99.69	9.62	89–92	180	2.77	506	0.00

Authors' compilation from the original operating bulletins.

All tests reached the same nominal maximum calcination temperature and had the same leach residence time, whereas sulfation-acid addition, calcination mass loss, final pH, ORP, and sulfurous-acid addition varied. The dataset is therefore interpreted as a screening matrix of coupled operating conditions, not as a one-factor experimental design.

2.5. Metal-balance reconciliation

For each element, the dissolved inventory was calculated from the combined final liquor and wash-water inventories. The solid inventory was calculated from the dry-residue mass and residue assay. Because analytical closures were not exactly 100%, the reconciled net transfer was calculated from the recovered-product inventories.

$$X_i,\text{rec} = m_i,\text{solution} / (m_i,\text{solution} + m_i,\text{residue}) \times 100 \quad (1)$$

where X_i,rec is the reconciled net transfer of element i, m_i, solution is the combined element mass in the liquor and wash solution, and m_i, residue is the element mass in the final dry residue. This metric expresses measured product partitioning and avoids interpreting analytical non-closure as extraction. It remains subject to sampling, assay, and unmeasured-process uncertainties.

2.6. Fe suppression and Fe-related stoichiometric acid liability

Iron suppression was defined as the complement of reconciled Fe transfer.

$$S_{Fe} = 100 - X_{Fe,rec} \quad (2)$$

The theoretical H_2SO_4 requirement for complete conversion and dissolution of feed Fe as Fe(III) sulfate was calculated using:

$$R_{Fe,100} = m_{Fe} \times (3/2) \times M_{H_2SO_4} / M_{Fe} \quad (3)$$

For 196 kg Fe/t ore, Equation (3) yields 516.34 kg H_2SO_4/t ore. The Fe-associated acid liability for test j was then calculated as:

$$R_{Fe,j} = R_{Fe,100} \times X_{Fe,j} / 100 \quad (4)$$

The difference $R_{Fe,100} - R_{Fe,j}$ is reported as a theoretical avoided Fe-related acid liability relative to complete ferric dissolution. It is not a measured saving relative to a conventional direct-leach control.

2.7. Reaction framework and mechanistic premises

The reaction framework was constructed from balanced limiting reactions and the thermal behavior described in the cited literature. The equations represent plausible pathways; they do not establish the actual phase sequence in the absence of stage-resolved XRD, sulfur speciation, and off-gas analysis.

$$2FeOOH + 3H_2SO_4 \rightarrow Fe_2(SO_4)_3 + 4H_2O \quad (5)$$

$$Fe_2O_3 + 3H_2SO_4 \rightarrow Fe_2(SO_4)_3 + 3H_2O \quad (6)$$

$$Fe_2(SO_4)_3 \rightarrow Fe_2O_3 + 3SO_3(g) \quad (7)$$

$$2FeSO_4 + 1/2O_2 \rightarrow Fe_2O_3 + 2SO_3(g) \quad (8)$$

$$CuO(eq) + SO_3(g) \rightarrow CuSO_4 \quad (9)$$

$$Fe_2(SO_4)_3 + 3CuO(eq) \rightarrow Fe_2O_3 + 3CuSO_4 \quad (10)$$

$$Fe_2(SO_4)_3 + 3MgO(eq) \rightarrow Fe_2O_3 + 3MgSO_4 \quad (11)$$

International Journal of Current Science Research and Review
ISSN: 2581-8341
Volume 09 Issue 07 July 2026
DOI: 10.47191/ijcsrr/V9-i7-59, Impact Factor: 8.048
IJCSRR @ 2026
www.ijcsrr.org

$Fe_2(SO_4)_3 + Al_2O_3(eq) \rightarrow Fe_2O_3 + Al_2(SO_4)_3$ (12)
$MnO_2 + SO_2(aq) \rightarrow MnSO_4(aq)$ (13)
$Fe_2O_3 + 6H^+ \rightarrow 2Fe^{3+} + 3H_2O$ (14)
$Fe^{3+} + 3H_2O \rightleftharpoons Fe(OH)_3(s) + 3H^+$ (15)

In Equations (9)–(12), oxide-equivalent notation represents a reactive metal-oxygen site formed in an oxide, hydroxide, partially dehydroxylated phyllosilicate, or amorphous reaction product. It does not imply that Cu, Mg, or Al occurred as discrete CuO, MgO, or Al_2O_3 in the original ore. Equations (7)–(12) describe two possible sulfate-redistribution pathways: release of SO_3 followed by gas-solid sulfation, and direct local sulfate exchange between ferric sulfate and a neighboring reactive site.

The relationship between the staged furnace program and the qualitative stability windows of Fe-, Al-, and Mg-bearing sulfates should be shown in Figure 2. The figure must be presented as a conceptual stability map rather than an experimentally measured phase diagram.

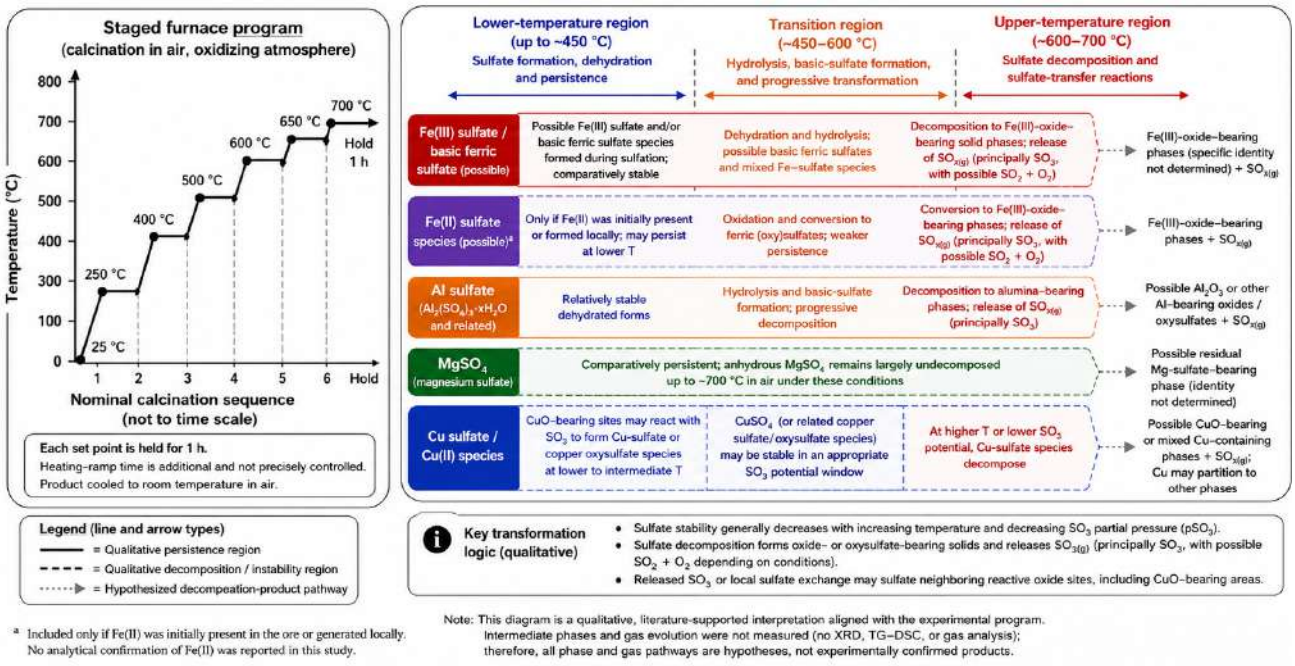

Figure 2. Schematic staged calcination profile and qualitative relative thermal behavior of $Fe_2(SO_4)_3$, $FeSO_4$-derived intermediates, $Al_2(SO_4)_3$, and $MgSO_4$ under oxidizing conditions.

Source: Authors' conceptual synthesis based on operating records and the thermal, kinetic, and thermodynamic literature cited in Sections 1.2–1.4 and 3.3–3.7.

The figure should show that ferric sulfate is expected to decompose within the upper calcination interval, that Al sulfate exhibits intermediate behavior, and that $MgSO_4$ remains relatively persistent at 700 °C. It should also show that insufficiently oxidizing conditions can preserve Fe(II)-sulfate or oxysulfate intermediates, thereby weakening Fe rejection.

2.8. Scope and statistical treatment

The six sulfation–calcination–leaching tests represented distinct operating conditions and were not independent experimental replicates. Each test was therefore treated as an observational unit ($n = 6$), and the statistical treatment was restricted to descriptive summaries, mass-balance consistency, and assessment of response robustness across the evaluated operating window. No estimate of analytical repeatability or experimental reproducibility was derived from variation among the six tests.

For each reconciled element-transfer variable, the arithmetic mean and sample standard deviation were calculated as supplementary descriptors of cross-condition dispersion:

International Journal of Current Science Research and Review
ISSN: 2581-8341
Volume 09 Issue 07 July 2026
DOI: 10.47191/ijcsrr/V9-i7-59, Impact Factor: 8.048
IJCSRR @ 2026
www.ijcsrr.org

$$\bar{x} = \frac{1}{n}\sum_{j=1}^{n} x_j \qquad (16)$$

$$s = \left[\frac{\sum_{j=1}^{n}(x_j - \bar{x})^2}{n-1}\right]^{1/2} \qquad (17)$$

where $x_j$is the reconciled transfer measured under operating condition j, $\bar{x}$ is the arithmetic mean, s is the sample standard deviation, and $n$is the number of distinct operating conditions. These statistics describe variation across the tested conditions and must not be interpreted as estimates of experimental uncertainty.

Because Fe transfer values were small, positively skewed, and influenced by the single highest-transfer condition, Fe suppression was evaluated primarily using the median, observed range, maximum Fe transfer, and corresponding minimum Fe suppression. Across the six distinct operating conditions, the median reconciled Fe transfer was 0.130%, with an observed range of 0.026–0.340%. The maximum observed transfer therefore provides a conservative demonstration that reconciled Fe transfer remained below 0.35% throughout the evaluated operating window. Equivalently, the minimum observed Fe suppression was 99.660%.

The calculated Fe-associated stoichiometric H_2SO_4 equivalents were summarized using the median, observed range, arithmetic mean, and standard deviation. These values represent calculated reagent-equivalent liabilities associated with the measured Fe partitioning, rather than direct measurements of acid consumption or reagent savings.

Results reported below the analytical limit of quantification for minor elements were treated as censored observations. No arbitrary midpoint, zero value, or quantification-limit substitution was introduced into the central Fe analysis.

No analysis of variance, t-test, regression significance test, confidence interval for treatment effects, or p-value was calculated. Sulfation-acid addition, calcination mass loss, final pH, oxidation–reduction potential, and sulfurous-acid addition varied simultaneously and were not arranged in an orthogonal experimental design. Consequently, differences among tests are interpreted as operational associations and as evidence supporting mechanistic hypotheses, rather than as statistically demonstrated causal effects.

Duplicated acid-soluble Cu assays available in the project archive were not included in the statistical treatment because Cu extraction was not the primary performance criterion for this study. The principal statistical endpoint was the robustness of low reconciled Fe transfer across the six evaluated operating conditions.

3. RESULTS AND DISCUSSION

3.1. The Fe-rich feed defines the correct performance criterion

The homogenized process feed contained 19.6 wt.% Fe and 1.05 wt.% Cu, corresponding to approximately 196 kg Fe and 10.5 kg Cu per tonne of dry ore. On a stoichiometric basis, complete conversion and dissolution of the feed Fe as Fe(III) sulfate would require approximately 516.34 kg H_2SO_4/t ore, according to:

$$Fe_2O_3 + 3H_2SO_4 \rightarrow Fe_2(SO_4)_3 + 3H_2O \qquad (18)$$

By comparison, complete conversion of the feed Cu to $CuSO_4$ would require approximately 16.21 kg H_2SO_4/t ore:

$$CuO + H_2SO_4 \rightarrow CuSO_4 + H_2O \qquad (19)$$

The ratio between the maximum theoretical Fe-related acid liability and the stoichiometric acid requirement associated with complete Cu sulfation was calculated as:

$$\frac{R_{Fe,100}}{R_{Cu,100}} = \frac{516.34}{16.21} \approx 31.85 \qquad (20)$$

Thus, the maximum theoretical Fe-related acid liability was approximately 32 times greater than the stoichiometric requirement associated with all Cu in the feed. This comparison does not imply that all Fe would dissolve during conventional atmospheric leaching. Rather, it defines the upper-bound acid burden associated with the large ferruginous inventory and demonstrates why net Fe transfer, rather than Cu extraction alone, is the appropriate primary performance criterion for the investigated route.

International Journal of Current Science Research and Review
ISSN: 2581-8341
Volume 09 Issue 07 July 2026
DOI: 10.47191/ijcsrr/V9-i7-59, Impact Factor: 8.048
IJCSRR @ 2026
www.ijcsrr.org

The representative mineralogical dataset for the oxidized-ore group supports this process rationale. Fe oxyhydroxides averaged 28.27 wt.%, while biotite and chlorite together averaged 40.61 wt.%. These modal values provide mineralogical context for the process feed but should not be interpreted as a direct modal analysis of the exact homogenized blend used in the six tests. Fe oxyhydroxides constitute the principal potential Fe-reactive reservoir, whereas biotite and chlorite are important potential sources of Mg and Al during acid treatment.

Direct atmospheric acid attack on this assemblage could therefore mobilize substantial quantities of Fe and other gangue-derived elements. The intended function of the sulfation–calcination–controlled-leaching sequence was not simply to increase acid strength or maximize overall mineral dissolution, but to exploit differences in sulfate formation, thermal stability, decomposition, and subsequent aqueous behavior. Accordingly, process effectiveness was assessed primarily by the ability to maintain a negligible Fe inventory in the final aqueous products while other acid-reactive elements remained measurably transferable.

3.2. Reconciled element transfer demonstrates selective Fe suppression

Table 4 compares the reconciled net transfers of Cu and gangue elements, highlighting the separation between Fe and other reactive elements.

Table 4. Reconciled net transfer of the principal elements to the combined liquor and wash solution.

Test	Cu (%)	Al (%)	Fe (%)	Mg (%)	Mn (%)	Si (%)
1	11.93	6.95	0.026	6.39	38.14	0.41
2	13.43	8.85	0.340	13.13	55.36	0.40
3	19.05	15.18	0.230	17.07	56.09	0.52
4	18.10	14.34	0.160	21.92	58.92	0.49
5	21.20	15.72	0.100	24.35	59.98	0.47
6	23.12	16.28	0.050	29.78	57.65	0.41

Authors' calculations based on feed, liquor, wash-water, and final-residue inventories. Values are screening-level reconciled product partitions, not statistically validated recoveries.

Fe transfer ranged from 0.026% to 0.340% across the six tests, corresponding to 99.660–99.974% Fe suppression. This result persisted over a tenfold range of sulfation-acid addition. By contrast, Mg transfer rose from 6.39% to 29.78%, Al reached 16.28%, and Mn remained between 38.14% and 59.98%. Consequently, the low Fe transfer cannot be explained by a general failure of leaching or by universal sulfate decomposition. It reflects element-specific chemistry.

The contrast should be shown in Figure 3 using a logarithmic or broken ordinate for Fe, or a secondary inset, because Fe transfer is two to three orders of magnitude lower than the responses for Mg, Mn, and Al.

International Journal of Current Science Research and Review
ISSN: 2581-8341
Volume 09 Issue 07 July 2026
DOI: 10.47191/ijcsrr/V9-i7-59, Impact Factor: 8.048
IJCSRR @ 2026
www.ijcsrr.org

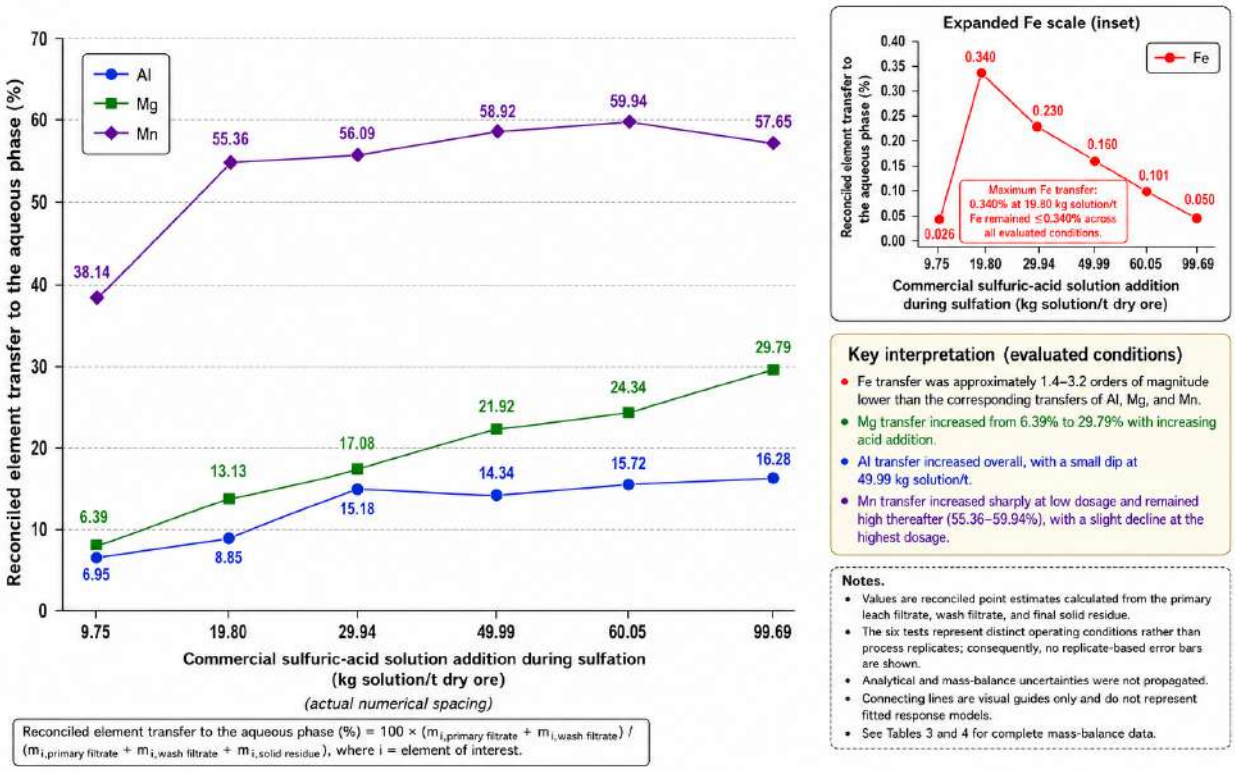

Figure 3. Reconciled net transfer of Fe, Al, Mg, and Mn as a function of sulfuric acid added during sulfation. Source: Authors' calculations based on the reconciled liquor, wash-water, and final-residue inventories summarized in Table 4.

The figure should make the central experimental result immediately clear: Fe remained below 0.35% throughout the matrix, whereas Mg and Al increased, and Mn remained high. This differential response is the primary evidence for selective Fe suppression.

3.3. Ferric-sulfate formation and decomposition provide the primary thermal barrier

The most plausible thermal sequence begins with the reaction of accessible Fe oxyhydroxide and oxide sites with sulfuric acid, as described in Equations (5) and (6). Low-temperature sulfation studies of iron oxides show that Fe reactivity depends on crystallinity, surface hydroxylation, acid concentration, and water activity (Gontijo et al., 2020). Basic ferric sulfate and related Fe(III) sulfate phases may also form as intermediate products (Ventruti et al., 2020).

As temperature increases, ferric sulfate becomes unstable and is converted to Fe_2O_3 while sulfur oxides are released. The present furnace endpoint of approximately 700 °C lies in a region where extensive decomposition is thermodynamically and kinetically plausible. Broader sulfate-roasting studies have repeatedly linked selective leaching to conversion of soluble Fe sulfates into less soluble Fe oxides during roasting or hematitization (Kart et al., 2021; Sun et al., 2026; Teixeira, 2020; Zhao et al., 2024).

The very low final Fe transfer is consistent with this transformation. Fe may transiently accept sulfate during the acid-mixing stage and then release sulfur oxides during calcination without remaining in the aqueous product. This role differs fundamentally from a simple inert-gangue model: Fe can participate in sulfur redistribution while being ultimately rejected as an oxide.

3.4. Internal sulfate redistribution may activate neighboring Cu-bearing sites

Equation (9) represents gas-solid sulfation by SO_3, while Equation (10) represents a limiting direct exchange between ferric sulfate and a CuO-equivalent site. Experimental use of iron sulfates as sulfating agents, thermodynamic simulations with Fe(III) sulfate, and selective roasting of Cu-bearing feeds support the plausibility of sulfate redistribution from Fe-bearing phases to valuable-metal sites (Grudinsky et al., 2021; Souza et al., 2022; Wan et al., 2020).

For the present ore, CuO(eq) should be understood as an accessible Cu-O coordination environment in an oxide, oxyhydroxide, Mn oxide, biotite, chlorite, or partially dehydroxylated reaction product. Heating can remove structural water, disrupt

International Journal of Current Science Research and Review
ISSN: 2581-8341
Volume 09 Issue 07 July 2026
DOI: 10.47191/ijcsrr/V9-i7-59, Impact Factor: 8.048
IJCSRR @ 2026
www.ijcsrr.org

phyllosilicate layers, and create reactive surfaces. Similar phase-specific behavior has been observed in laterites, serpentines, slags, and mattes, where the mineral host determines whether the sulfate product remains soluble after roasting (Hariyanto et al., 2023a; Ribeiro et al., 2021; Sun et al., 2020; Xiao et al., 2021).

The measured Cu transfer of 11.93–23.12% indicates that sulfate redistribution, if it occurred, was incomplete. Possible causes include limited physical contact, encapsulation, refractory Cu in silicate structures, decomposition of Cu sulfate at the highest local temperatures, or reprecipitation during leaching. Because Cu optimization is outside the scope of this paper, these possibilities are used only to constrain the Fe-suppression mechanism.

3.5. An oxidizing furnace atmosphere is a necessary process condition

Equation (8) illustrates why oxygen availability is essential. $FeSO_4$-derived intermediates must be oxidized toward Fe(III) oxide if the process is to avoid persistence of comparatively stable Fe(II)-sulfate or oxysulfate phases. High-temperature studies of melanterite, global kinetic analysis of $FeSO_4$ decomposition, and oxidation studies of sulfide and sulfate-bearing materials show that the reaction sequence is strongly gas-dependent (Lacalamita et al., 2021; Klyushnikov et al., 2021, 2023; Rego et al., 2024).

In an oxidizing atmosphere, Fe(II) generated locally by mineral reactions or partial sulfate reduction can be driven toward Fe(III) oxide while sulfur is released as SO_2/SO_3. In oxygen-deficient regions, Fe(II)-bearing intermediates may persist, delay sulfur release, or dissolve during the subsequent leach. Therefore, scale-up should use controlled air or oxygen flow, shallow beds or effective solids mixing, and off-gas monitoring rather than relying on nominally oxidative furnace conditions.

Thermodynamic and experimental roasting studies of multimetal feeds further indicate that oxygen and sulfur potentials jointly control the stability fields of Fe, Cu, Co, and Ni sulfates and oxides (Sun et al., 2026; Urtnasan et al., 2024; Wan et al., 2021; Zhang et al., 2026). The present results are consistent with an oxidizing route, but the original records do not provide direct gas-composition evidence.

3.6. pH-controlled leaching provides a second Fe-rejection barrier

Calcination alone does not guarantee a low-Fe liquor because residual ferric sulfate, amorphous Fe phases, or newly formed high-surface-area Fe_2O_3 can still dissolve. The subsequent leach was operated at approximately 90 °C, with final PLS pH values of 2.33–2.77. Under these conditions, Fe(III) hydrolysis and precipitation can limit net Fe accumulation even if some transient dissolution occurs.

The broader iron-removal literature shows that goethite, hematite, jarosite, basic ferric sulfate, and poorly crystalline Fe(III) products form over overlapping pH-temperature-redox windows (Buriti et al., 2024, 2025; Cruells & Roca, 2022; da Silva et al., 2022; Das & Li, 2023; Deng et al., 2020; Febriana et al., 2026). These studies do not identify the specific Fe product in the present residues, but they support the premise that controlled pH can provide an aqueous rejection barrier after the thermal stage.

The combined route is therefore more robust than either stage alone. Calcination reduces the inventory of soluble Fe sulfate and regenerates Fe oxide; controlled-pH leaching limits renewed oxide attack and promotes hydrolysis of any Fe(III) entering solution. The measured Fe transfer is the net result of both barriers.

3.7. Quantified Fe suppression and acid-liability reduction

Table 5 converts the measured Fe transfer into the corresponding stoichiometric H_2SO_4 liability. The calculation expresses the process benefit in reagent-equivalent terms, avoiding market prices or a full economic model.

Table 5. Fe suppression and theoretical Fe-related sulfuric-acid liability.

Test	Net Fe transfer (%)	Fe suppression (%)	Fe-associated H_2SO_4 (kg/t)	Potential avoided Fe acid liability (kg/t)
1	0.026	99.974	0.134	516.206
2	0.340	99.660	1.756	514.584
3	0.230	99.770	1.188	515.152
4	0.160	99.840	0.826	515.514
5	0.100	99.900	0.516	515.824
6	0.050	99.950	0.258	516.082
Mean	0.151	99.849	0.780	515.560

International Journal of Current Science Research and Review
ISSN: 2581-8341
Volume 09 Issue 07 July 2026
DOI: 10.47191/ijcsrr/V9-i7-59, Impact Factor: 8.048
IJCSRR @ 2026
www.ijcsrr.org

Authors' calculations. The complete-ferric-dissolution reference is 516.34 kg H_2SO_4 per ton of ore. "Potential avoided" is a stoichiometric upper bound, not a measured saving relative to direct atmospheric leaching.

The measured Fe transfer was only 0.13–1.76 kg H_2SO_4/t ore, with a mean of approximately 0.78 kg/t. Relative to complete ferric dissolution, the theoretical avoided Fe-related acid liability was 514.58–516.21 kg/t. This magnitude demonstrates why Fe suppression can dominate acid-use efficiency in a 19.6 wt.% Fe ore.

This upper-bound comparison must not be interpreted as an experimentally demonstrated saving of approximately 516 kg/t relative to conventional leaching. Direct atmospheric leaching would not necessarily dissolve all Fe, and the actual comparison depends on temperature, pH, acid activity, mineralogy, and residence time. A matched direct-leach control is needed to quantify the actual reduction in acid consumption. Nevertheless, the calculation rigorously shows that the measured final Fe inventory carried only a negligible fraction of the feed's maximum ferric-acid liability.

Figure 4 compares the complete-ferric-dissolution reference with the calculated Fe-associated stoichiometric acid equivalents for the six operating conditions. A logarithmic main panel and an expanded linear inset are used to preserve visibility of the low test values.

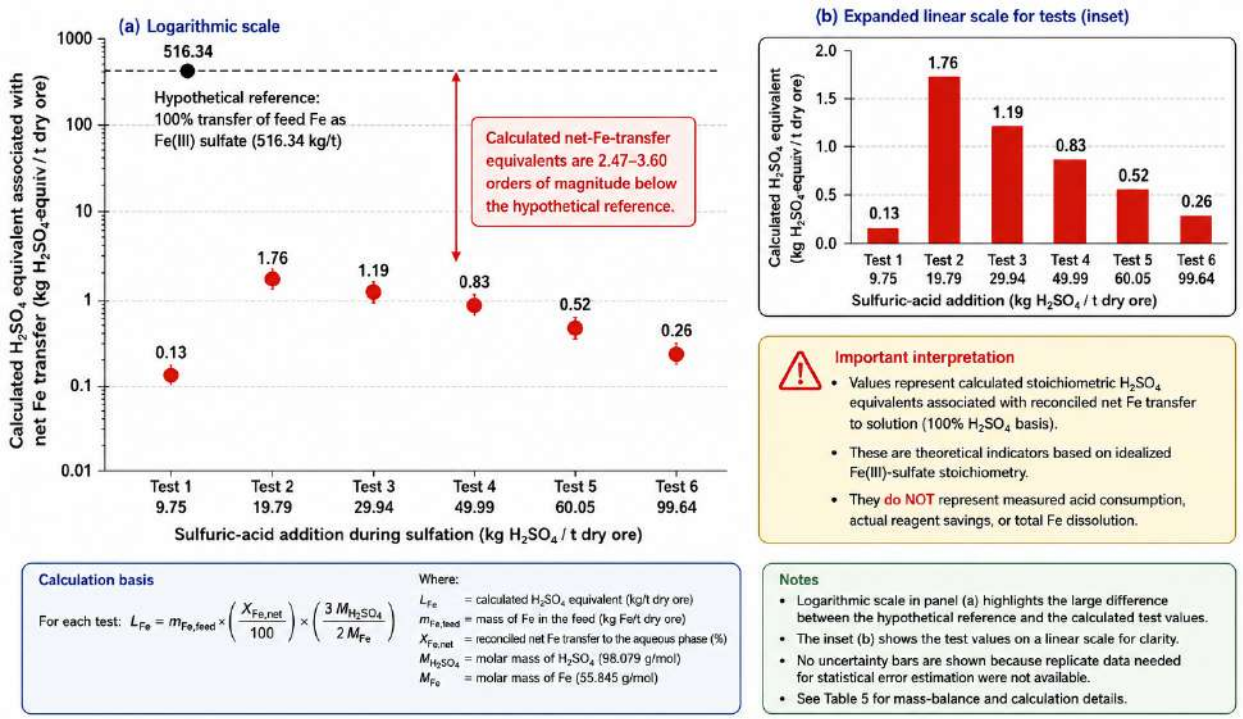

Figure 4. Theoretical Fe-related H_2SO_4 liability for complete ferric dissolution, compared with liabilities associated with measured Fe transfer across the six tests.

Source: Authors' calculations based on the feed Fe content, Fe(III)-sulfate stoichiometry, and reconciled Fe transfers reported in Table 5.

The logarithmic comparison shows that the calculated Fe-associated acid equivalents were 2.47–3.60 orders of magnitude below the complete-ferric-dissolution reference. These values are theoretical stoichiometric equivalents and must not be interpreted as measured acid consumption or actual reagent savings.

3.8. Mg was not suppressed because $MgSO_4$ behaved as a stable sulfate sink

Mg transfer increased from 6.39% to 29.78% as sulfation-acid addition increased. This response is consistent with progressive attack on reactive Mg-bearing sites in biotite and chlorite and with the formation of soluble $MgSO_4$. Unlike ferric sulfate, $MgSO_4$ is comparatively persistent under the applied calcination conditions. Magnesium extraction and sulfate-crystallization

International Journal of Current Science Research and Review
ISSN: 2581-8341
Volume 09 Issue 07 July 2026
DOI: 10.47191/ijcsrr/V9-i7-59, Impact Factor: 8.048
IJCSRR @ 2026
www.ijcsrr.org

studies demonstrate that Mg tends to remain associated with sulfate once mobilized (Peng et al., 2021; Reddy et al., 2020; Wanderley et al., 2020; Yang et al., 2022).

Equation (11) is therefore thermodynamically plausible as a sulfate-transfer endpoint but not as a beneficial donor cycle. Ferric sulfate or SO_3 may sulfate an Mg-bearing oxide-equivalent site, after which $MgSO_4$ retains the sulfate through calcination and dissolves during leaching. In this sense, Mg acts as a sulfate sink. The process suppresses Fe but not Mg because the sulfate stability ordering differs. Reviews of mineral-based Mg extraction and studies of serpentinite-acid interaction support this interpretation (Taheri & Larachi, 2025; Yeskibayeva et al., 2024).

3.9. Mn was not suppressed because its aqueous response was redox-sensitive

Mn transfer remained high at 38.14–59.98%, despite the low modal abundance of Mn oxides. Sulfurous acid was added in Tests 1–5, and Equation (13) represents a simplified reductive dissolution pathway by which Mn(IV) oxide can be converted to soluble Mn(II) sulfate. Variations in ORP and reductant addition therefore confound any attempt to attribute Mn transfer solely to the sulfation or calcination stage.

The high Mn response provides valuable mechanistic evidence: the route did not generally passivate all oxides. Fe suppression arose from Fe-specific sulfate decomposition and aqueous hydrolysis chemistry, whereas Mn remained susceptible to redox-assisted dissolution. Future experiments should hold ORP and the addition of sulfurous acid constant if Mn behavior is to be modeled independently.

3.10. Al showed intermediate sulfate behavior

Al transfer increased from 6.95% to 16.28%, with most of the increase occurring by Test 3 and a plateau near 14–16% thereafter. Complete sulfation and dissolution of the feed Al would require approximately 292.8 kg H_2SO_4/t ore, so even moderate Al transfer can impose a significant acid burden.

The Al response is consistent with an intermediate thermal window. Aluminum sulfate and alum-type phases dehydrate and decompose over broad temperature ranges that depend on structure, atmosphere, and heating rate (Rego et al., 2021; Zheng et al., 2020). Thermal activation of alunite and ammonium-sulfate roasting of Al-rich feeds further indicate that Al and sulfur can partition differently depending on the phase assemblage and temperature history (Chen et al., 2026; Xu et al., 2022).

Equation (12) therefore represents a plausible but incomplete sulfate-transfer pathway. Some Al-bearing sites may accept sulfate from ferric sulfate or SO_3; some Al sulfate may decompose during the upper calcination interval; and refractory Al may remain in biotite, chlorite, garnet, kaolinite, or other aluminosilicates. The observed plateau may reflect exhaustion of the most reactive Al sites, counterbalanced by decomposition or retention of less reactive Al phases. Stage-resolved mineralogy and sulfur analysis are required to distinguish among these possibilities.

3.11. Metal-associated sulfate demand confirms that Fe was decoupled from the liquor

Table 6 allocates stoichiometric H_2SO_4 equivalents associated with the measured transfers of Cu, Al, Fe, Mg, and Mn. This is not an operating acid-consumption balance; it is a product-based allocation of sulfate equivalents.

Table 6. Stoichiometric H_2SO_4 equivalents associated with measured metal transfer.

Test	Cu	Al	Fe	Mg	Mn	Total
1	1.93	20.35	0.13	3.79	3.57	29.77
2	2.18	25.91	1.76	7.79	5.18	42.81
3	3.09	44.45	1.19	10.13	5.24	64.09
4	2.93	41.99	0.83	13.00	5.51	64.26
5	3.44	46.03	0.52	14.44	5.61	70.03
6	3.75	47.67	0.26	17.67	5.39	74.73

Authors' calculations. Values are in kg H_2SO_4 per t of dry ore and are based on sulfate stoichiometry for Cu(II), Al(III), Fe(III), Mg(II), and Mn(II).

International Journal of Current Science Research and Review
ISSN: 2581-8341
Volume 09 Issue 07 July 2026
DOI: 10.47191/ijcsrr/V9-i7-59, Impact Factor: 8.048
IJCSRR @ 2026
www.ijcsrr.org

Fe contributed only a negligible fraction of the measured metal-associated sulfate demand. Al dominated, Mg increased with acid addition, and Mn remained significant. The general sequence was Al ≫ Mg > Mn > Cu ≫ Fe. This ordering confirms that the process decoupled the large Fe inventory from the final liquor but did not eliminate sulfate consumption by other reactive phases.

The difference between applied acid and product-based sulfate equivalents includes free acid, sulfate retained in the residue, unmeasured minor elements, protonation or partial dissolution of silicates, sulfur-oxide losses, precipitation-redissolution cycles, and analytical uncertainty. A complete sulfur balance would be required to close the reagent inventory.

3.12. Integrated mechanism of Fe suppression

The combined evidence supports a two-barrier Fe-suppression mechanism within a three-stage process. During sulfation, accessible Fe oxyhydroxide and oxide sites can form Fe(III) sulfate or basic ferric sulfate. During oxidative calcination, Fe sulfate decomposes, regenerating Fe_2O_3 and releasing SO_3/SO_2. Sulfur oxides or direct local exchange may sulfate nearby reactive Cu-, Mg-, or Al-bearing oxide-equivalent sites. During pH-controlled leaching, soluble sulfates dissolve, regenerated Fe_2O_3 remains poorly soluble, and any Fe(III) entering solution is susceptible to hydrolysis or precipitation.

The proposed mechanism is consistent with the measured elemental partitioning and with the literature on iron sulfate reactivity, sulfate roasting, Fe precipitation, and sulfate stability. It is also consistent with the observation that Mg and Mn were not suppressed: Mg retained sulfate as stable $MgSO_4$, whereas Mn remained responsive to redox-assisted leaching. Al occupied an intermediate position.

The integrated working mechanism should be summarized in Figure 5. The drawing must clearly label the mechanism as a hypothesis constrained by mass balances and published chemistry, rather than as a directly observed phase sequence.

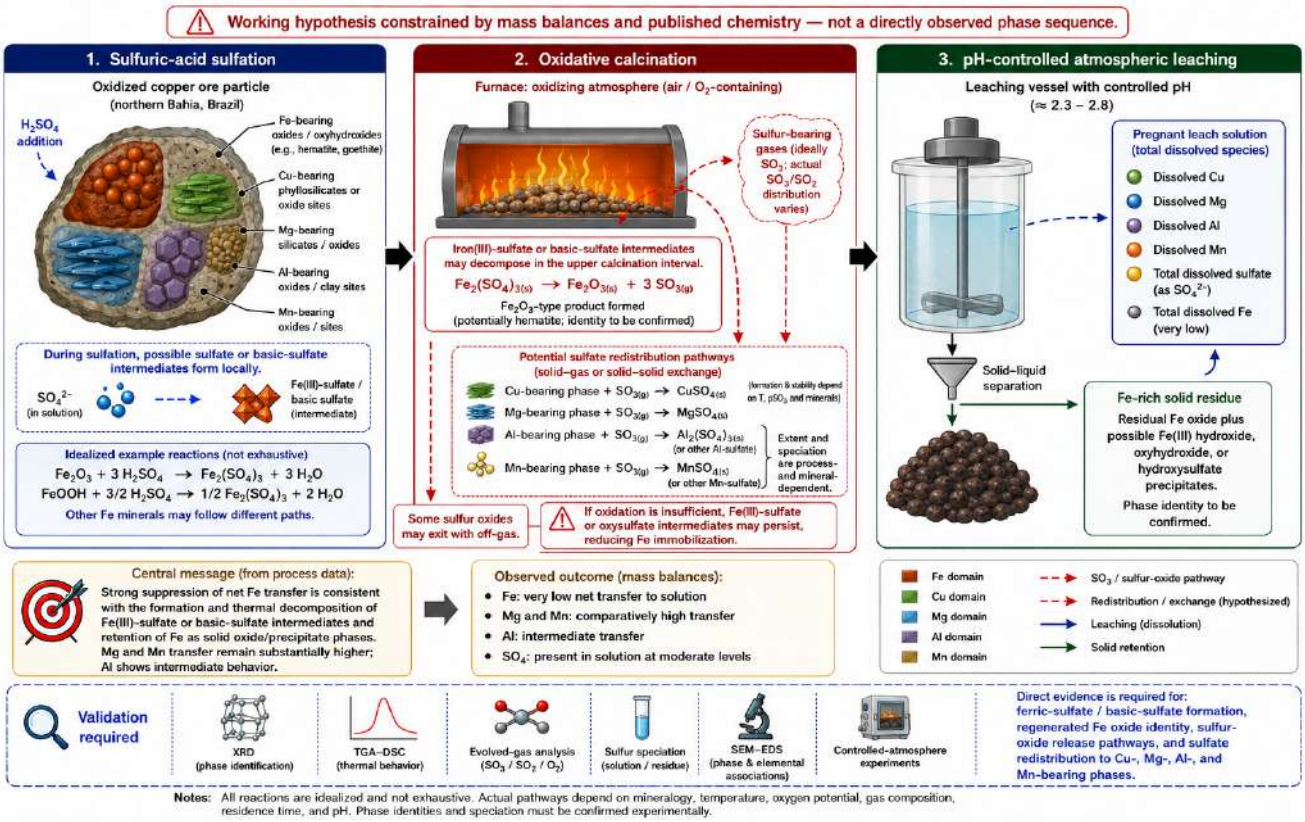

Figure 5: illustrates the proposed mechanism for Fe suppression during sulfuric-acid sulfation, oxidative calcination, and pH-controlled leaching. Ferric sulfate breaks down into Fe_2O_3 and sulfur oxides; SO_3 or local exchange may sulfate Cu-, Mg-, or Al-sites; pH control dissolves soluble sulfates while limiting Fe transfer.

Source: Authors' model, based on Equations (5)–(15), data, and literature.

International Journal of Current Science Research and Review
ISSN: 2581-8341
Volume 09 Issue 07 July 2026
DOI: 10.47191/ijcsrr/V9-i7-59, Impact Factor: 8.048
IJCSRR @ 2026
www.ijcsrr.org

The mechanism should be validated using XRD, TGA–DSC, evolved-gas analysis, sulfur speciation, SEM–EDS, and controlled-atmosphere experiments. In particular, direct evidence is required for ferric-sulfate formation, the identity of the regenerated Fe oxide, the sulfur-oxide release interval, and any sulfate redistribution to Cu-bearing phyllosilicates or oxide phases.

3.13. Relationship to broader sulfation-roasting research

The present study differs from many sulfation-roasting investigations because its primary success criterion is not maximizing valuable-metal extraction but suppressing a dominant impurity. Nevertheless, the findings align with broader evidence that roasting selectivity depends on phase transformation, sulfate stability, and mineral host. Laterite studies have documented valuable-metal losses, selective extraction windows, and the influence of MgO, SiO_2, salts, and mineralogy (Hariyanto et al., 2023a, 2023b, 2024; Ribeiro et al., 2020, 2021, 2022; Zhao et al., 2024, 2025b). Studies of REE ores, bauxite residues, slags, and silicate feeds show similar sensitivity to acid baking, roasting temperature, and reaction-rim development (Bian et al., 2020; Falah et al., 2026; Gontijo et al., 2023; Maluleke et al., 2023; Thibault et al., 2026).

The literature also shows that alternative acid systems or coproduced Fe phases can be used to manage ferruginous feeds, but these approaches target different process objectives (Xiao et al., 2026). The present work makes a narrower, more direct contribution: it demonstrates that sulfation, oxidative calcination, and controlled-pH leaching can keep Fe transfer below 0.35% even when the feed contains 19.6 wt.% Fe.

3.14. Limitations and validation priorities

The main limitation is the absence of a matched direct-leaching control. The study quantifies Fe suppression within the combined route but cannot isolate the actual acid saving relative to conventional atmospheric leaching. A direct-leach control should use the same ore, solids concentration, temperature, residence time, pH trajectory, and redox conditions.

The second limitation is the lack of independent replicates for the six main conditions. Future work should repeat the low-, intermediate-, and high-acid sulfation conditions and report confidence intervals for Fe transfer and acid liability.

The third limitation is the lack of phase- and sulfur-resolved measurements. XRD, automated mineralogy, SEM–EDS, total sulfur, sulfate sulfur, TGA–DSC, and evolved-gas analysis should be applied to the feed, sulfated material, intermediate calcines, final calcine, and leach residue. These measurements would test the assumed ferric-sulfate pathway and quantify sulfate redistribution.

Finally, the furnace atmosphere and leach ORP should be controlled independently. A factorial design that varies oxygen partial pressure, calcination temperature, sulfation-acid dosage, final pH, and ORP would directly test the roles of $FeSO_4$ oxidation, $Fe_2(SO_4)_3$ decomposition, SO_3 transfer, and Fe(III) hydrolysis.

4. CONCLUSIONS

Across six distinct operating conditions, the integrated sulfuric-acid sulfation, oxidative calcination, and pH-controlled atmospheric leaching route maintained a reconciled Fe transfer between 0.026% and 0.340% from an oxidized copper ore containing 19.6 wt.% Fe. This corresponds to Fe suppression of approximately 99.66–99.97%. The response was selective because Mg, Mn, and Al exhibited substantially greater aqueous transfer, demonstrating that the low Fe transfer did not result from a general inhibition of mineral dissolution.

The measured Fe transfers corresponded to calculated stoichiometric acid equivalents of only 0.13–1.76 kg H_2SO_4/t ore. By comparison, hypothetical complete conversion and dissolution of the feed Fe as Fe(III) sulfate would require approximately 516.34 kg H_2SO_4/t ore. This difference quantifies the upper-bound Fe-related acid liability avoided by retaining Fe outside the final aqueous products. It does not represent an experimentally measured reagent saving, because a matched direct-leaching control was not included.

The observed behavior is consistent with initial formation of ferric sulfate, basic ferric sulfate, or related Fe-bearing sulfate intermediates during sulfation, followed by their thermal destabilization and conversion to poorly soluble Fe(III)-oxide-bearing phases during calcination. Sulfur oxides released during this transformation, particularly SO_3, may have promoted the sulfation of neighboring reactive metal–oxygen sites, including sites generated by dehydroxylation or partial structural disruption of Cu-bearing biotite, chlorite, Mn oxides, or other phases. An oxidizing furnace atmosphere is expected to favor Fe(III)-oxide formation and

International Journal of Current Science Research and Review
ISSN: 2581-8341
Volume 09 Issue 07 July 2026
DOI: 10.47191/ijcsrr/V9-i7-59, Impact Factor: 8.048
IJCSRR @ 2026
www.ijcsrr.org

reduce the persistence of Fe(II)-sulfate or oxysulfate intermediates, although the furnace gas composition and intermediate phases were not measured directly.

Leaching at approximately 90 °C and final pH values of 2.33–2.77 was consistent with an additional aqueous Fe-rejection barrier by limiting renewed attack on Fe-rich solids and favoring hydrolysis or reprecipitation of any Fe(III) released. The individual contributions of calcination and pH control could not, however, be isolated experimentally. Mg transfer increased to 29.78%, consistent with $MgSO_4$ acting as a comparatively persistent sulfate sink, while Mn transfer remained between 38.14% and 59.98% because of its redox-sensitive dissolution behavior. Al exhibited intermediate transfer of 6.95–16.28%, compatible with partial sulfate formation, thermal decomposition, and retention in less reactive aluminosilicate phases.

The principal contribution of this study is the quantitative demonstration that a coupled sulfation–calcination–controlled-leaching route can strongly suppress net Fe transfer from a highly ferruginous oxidized ore while other reactive elements remain mobile. The proposed phase transformations and sulfate-redistribution pathways remain working hypotheses supported by reconciled mass balances and established sulfate chemistry. Their confirmation requires stage-resolved mineralogy, sulfur speciation, thermal analysis, off-gas monitoring, controlled-atmosphere calcination, and direct-leaching controls.

DECLARATIONS

Funding

No external funding was received for the preparation of this manuscript. The original experimental work was conducted within an industrial mineral-processing research program.

Conflict of Interest

The author declares no conflict of interest.

Data Availability

The operating records, analytical certificates, mineralogical dataset, and calculation worksheets supporting this study are available from the corresponding author upon reasonable request, subject to applicable ownership and confidentiality restrictions.

Author Contributions

Antonio Clareti Pereira: Conceptualization; methodology; investigation; formal analysis; data curation; visualization; writing—original draft; writing—review and editing.

REFERENCES

1. Bian, Z.-Z., Feng, Y.-L., & Li, H.-R. (2020). Extraction of valuable metals from Ti-bearing blast furnace slag using ammonium sulfate pressurized pyrolysis–acid leaching processes. *Transactions of Nonferrous Metals Society of China, 30*(10), 2836–2847. https://doi.org/10.1016/S1003-6326(20)65425-5
2. Buriti, M. de S., Cézac, P., & Casás, L. (2024). Dissolution and precipitation of jarosite-type compounds: State of the art and future perspectives. *Comptes Rendus Chimie, 27*(S4), 81–109. https://doi.org/10.5802/crchim.321
3. Buriti, M. de S., Poulain, M., Cézac, P., & Casás, L. (2025). K-jarosite precipitation kinetics at low-moderate temperatures: Factors affecting mechanism, formation rates, solid morphology and crystallinity. *Hydrometallurgy, 235*, Article 106474. https://doi.org/10.1016/j.hydromet.2025.106474
4. Chen, Y., Liao, Y., Yu, D., Guo, X., Zhang, L., & Tian, Q. (2026). Thermal activation of hydronium alunite for selective leaching of Al and S from HPAL residue. *Journal of Sustainable Metallurgy, 12*(2), 2270–2283. https://doi.org/10.1007/s40831-026-01460-9
5. Cruells, M., & Roca, A. (2022). Jarosites: Formation, structure, reactivity and environmental. *Metals, 12*(5), Article 802. https://doi.org/10.3390/met12050802
6. da Silva, M. de F., de Sousa Oliveira, M. R., dos Santos, I. D., Radino-Rouse, P., & Mansur, M. B. (2022). Iron precipitation strategies from nickel laterite ore sulfuric acid leach liquor. *Mineral Processing and Extractive Metallurgy Review, 43*(1), 28–39. https://doi.org/10.1080/08827508.2020.1809392
7. Das, G. K., & Li, J. (2023). Iron removal as goethite from synthetic laterite leach solutions. *ACS Omega, 8*(13), 11931–11940. https://doi.org/10.1021/acsomega.2c07595

International Journal of Current Science Research and Review
ISSN: 2581-8341
Volume 09 Issue 07 July 2026
DOI: 10.47191/ijcsrr/V9-i7-59, Impact Factor: 8.048
IJCSRR @ 2026
www.ijcsrr.org

8. Deng, Z.-G., Yang, F., Wei, C., Zhu, B.-P., Zeng, P., Li, X.-B., Li, C.-X., & Li, M.-T. (2020). Transformation behavior of ferrous sulfate during hematite precipitation for iron removal. *Transactions of Nonferrous Metals Society of China, 30*(2), 492–500. https://doi.org/10.1016/S1003-6326(20)65229-3
9. Dickson, O. V., Deleau, T., Espitalier, F., Coquelet, C., Lombart, J., & Nallet, V. (2026). Autoclave scaling behaviour and characterisation during nickel laterite ore leaching under HPAL conditions. *Cleaner Waste Systems, 14*, Article 100503. https://doi.org/10.1016/j.clwas.2026.100503
10. Dong, B., Tian, Q., Guo, X., Wang, Q., Xu, Z., & Li, D. (2022). Leaching behavior of scandium from limonitic laterite ores under sulfation roasting–water leaching. *Journal of Sustainable Metallurgy, 8*(3), 1078–1089. https://doi.org/10.1007/s40831-022-00551-7
11. Dong, B., Tian, Q., Xu, Z., Guo, X., Wang, Q., & Li, D. (2023). The effect of pre-roasting on atmospheric sulfuric acid leaching of saprolitic laterites. *Hydrometallurgy, 218*, Article 106063. https://doi.org/10.1016/j.hydromet.2023.106063
12. Falah, F. N., Kurniawan, K., Ichlas, Z. T., & Mubarok, M. Z. (2026). Recovery of scandium from bauxite residue using sulfation roasting-assisted water leaching process. *Mineral Processing and Extractive Metallurgy Review, 47*(2), 211–225. https://doi.org/10.1080/08827508.2025.2454694
13. Febriana, E., Hidayat, T., Fauzi, I., Irawan, J., Mayangsari, W., Rhamdani, A. R., Prasetyo, A. B., Oediyani, S., & Firdiyono, F. (2026). Iron removal from acidic limonitic laterite leach solution through controlled oxidative and alkaline precipitation. *Mining, Metallurgy & Exploration, 43*, 2823–2832. https://doi.org/10.1007/s42461-026-01548-6
14. Gayratov, B., Gayratov, B., Godirilwe, L. L., Danha, G., & Shibayama, A. (2026). Waste-on-waste roasting of copper slag with flotation tailings for selective recovery of Cu, Ni, and Co. *Recycling, 11*(7), Article 124. https://doi.org/10.3390/recycling11070124
15. Gontijo, V. L., Teixeira, L. A. V., & Ciminelli, V. S. T. (2020). The reactivity of iron oxides and hydroxide during low-temperature sulfation. *Hydrometallurgy, 197*, Article 105452. https://doi.org/10.1016/j.hydromet.2020.105452
16. Gontijo, V. L., Teixeira, L. A. V., & Ciminelli, V. S. T. (2023). The effect of iron- and calcium-rich waste rock's acid baking conditions on the rare-earth extraction. *Minerals, 13*(2), Article 217. https://doi.org/10.3390/min13020217
17. Grudinsky, P. I., Zhiltsova, E. E., Grigorieva, D. D., & Dyubanov, V. G. (2021). Experimental study of the sulphatizing roasting of flotation tailings from copper slag processing using iron sulfates. *IOP Conference Series: Earth and Environmental Science, 666*(2), Article 022046. https://doi.org/10.1088/1755-1315/666/2/022046
18. Hariyanto, R. K. S., da Rocha, L. T., Kim, S.-J., & Jung, S.-M. (2023a). Extraction behavior of nickel and cobalt from serpentine-rich ore through sulfation–roasting–leaching process. *Metallurgical and Materials Transactions B, 54*(6), 2915–2928. https://doi.org/10.1007/s11663-023-02934-x
19. Hariyanto, R. K. S., da Rocha, L. T., Kim, S.-J., & Jung, S.-M. (2023b). Influence of alkali salts on extraction of nickel from serpentine-rich ore through sulfation roasting leaching process. *Journal of Sustainable Metallurgy, 9*(4), 1636–1646. https://doi.org/10.1007/s40831-023-00753-7
20. Hariyanto, R. K. S., da Rocha, L. T., Cho, S.-K., & Jung, S.-M. (2024). Influence of SiO_2 and MgO on extraction of nickel and cobalt from laterite ores by sulfation roasting leaching process. *Metallurgical and Materials Transactions B, 55*(3), 1455–1470. https://doi.org/10.1007/s11663-024-03039-9
21. Kart, E. U., Yazğan, Z. H., & Gümüşsoy, A. (2021). Investigation of iron selectivity behaviour of copper smelter slag flotation tailing with hematitization baking and base metals leaching methods. *Physicochemical Problems of Mineral Processing, 57*(5), 164–175. https://doi.org/10.37190/ppmp/141947
22. Klyushnikov, A. M., Gulyaeva, R. I., Selivanov, E. N., & Pikalov, S. M. (2021). Kinetics and mechanism of oxidation for nickel-containing pyrrhotite tailings. *International Journal of Minerals, Metallurgy and Materials, 28*(9), 1469–1477. https://doi.org/10.1007/s12613-020-2109-x
23. Klyushnikov, A. M., Pikalov, S. M., & Gulyaeva, R. I. (2023). Kinetics of solid-state oxidation of iron, copper and zinc sulfide mixture. *Chimica Techno Acta, 10*(2), Article 202310202. https://doi.org/10.15826/chimtech.2023.10.2.02
24. Kutluata, O. B., & Obut, A. (2026). Leaching behaviour of scandium from a clayey laterite ore in sulfuric acid solutions. *Physicochemical Problems of Mineral Processing, 62*(1), Article 218081. https://doi.org/10.37190/ppmp/218081

International Journal of Current Science Research and Review
ISSN: 2581-8341
Volume 09 Issue 07 July 2026
DOI: 10.47191/ijcsrr/V9-i7-59, Impact Factor: 8.048
IJCSRR @ 2026
www.ijcsrr.org

25. Lacalamita, M., Ventruti, G., Della Ventura, G., Radica, F., Mauro, D., & Schingaro, E. (2021). In situ high-temperature X-ray powder diffraction and infrared spectroscopic study of melanterite, $FeSO_4 \cdot 7H_2O$. *Minerals, 11*(4), Article 392. https://doi.org/10.3390/min11040392
26. Maluleke, K. C., Goso, X. C., Ndlovu, S., & Matinde, L. (2023). Investigations into the extraction of rare earth elements from Zandkopsdrift ore using the sulfation roasting process. *Minerals Engineering, 191*, Article 107902. https://doi.org/10.1016/j.mineng.2022.107902
27. Mamyrbayeva, K., Kuandykova, A., Chepushtanova, T., Merkibayev, Y., & Mishra, B. (2026). Investigation of the sulfation-roasting-water leaching process for efficient recovery of nickel and cobalt from Kazakhstan's laterite ore. *Canadian Metallurgical Quarterly, 65*(3), 1–16. https://doi.org/10.1080/00084433.2025.2603070
28. Muhammad, A. J., Nakagawa, K., Karya, I. P. A., Ndita, A., Darusman, L. O. M., Iwamoto, T., Terui, Y., Agusu, L., Sudiana, I. N., Nishimura, F., Nishiumi, T., Asano, T., Kikuchi, H., & Mitsudo, S. (2025). Microwave-assisted roasting-leaching of nickel from Indonesian nickel laterite ore. *International Journal of Acta Material, 1*(2), 73–83. https://doi.org/10.62749/ijactmat.v1i2.10
29. Osali, M., Ahani, F., Aboutalebi, M. R., Adeli, M., Moghaddam, J., Karimi, S., Wijenayake, J. J., & Alagha, L. (2026). Selective extraction of nickel and cobalt from limonitic laterite via optimized sulfation roasting–water leaching and solvent extraction. *Minerals, 16*(5), Article 431. https://doi.org/10.3390/min16050431
30. Peng, X., Liu, W., Liu, W., Zhao, L., Zhang, N., Gu, X., & Zhou, S. (2021). Fluorite-enhanced magnesium recovery from serpentine tailings: Kinetics and reaction mechanisms. *Hydrometallurgy, 201*, Article 105571. https://doi.org/10.1016/j.hydromet.2021.105571
31. Pereira, A. C. (2026a). Balancing nickel recovery, iron dissolution, acid dosage, and residence time in atmospheric sulfuric acid leaching of a ferruginous lateritic nickel ore. *Journal International Review of Research Studies, 1*(9), 1–30. https://doi.org/10.66104/dempc459.
32. Pereira, A. C. (2026b). From mineralogy to process design: The role of particle size distribution on nickel extraction kinetics and hydrometallurgical route selection in a limonitic laterite. *IKR Journal of Engineering and Technology, 2*(4), 1–17. https://doi.org/10.5281/zenodo.21209619.
33. Qin, H., Liu, P., Yu, D., Li, T., & Tian, Q. (2026). Nickel extraction from ferronickel alloy via sulfuric acid curing–oxidative decomposition roasting followed by water leaching. *JOM, 78*(7), 6793–6805. https://doi.org/10.1007/s11837-026-08355-w
34. Reddy, K. V. K., Sanjana, V., Singh, V., & Kapure, G. (2020). Processing of peridotite rocks of chromite ore overburden into magnesium salts and micro silica. *Mining, Metallurgy & Exploration, 37*(4), 1253–1263. https://doi.org/10.1007/s42461-020-00211-y
35. Rego, A. S. C., Marprates, C. V. B., Silva, T. S. X., Neto, J. G., Navarro, R. C. S., Souza, R. F. M., & Brocchi, E. A. (2021). $KAl(SO_4)_2$ thermal decomposition kinetics modeling through graphical and PSO methods. *Journal of Materials Research and Technology, 14*, 1975–1984. https://doi.org/10.1016/j.jmrt.2021.07.086
36. Rego, A. S. C., Navarro, R. C. S., Brocchi, E. A., & Souza, R. F. M. (2024). Kinetic study on the thermal decomposition of iron(II) sulfate using a global optimization approach. *Materials Chemistry and Physics, 327*, Article 129869. https://doi.org/10.1016/j.matchemphys.2024.129869
37. Ribeiro, P. P. M., de Souza, L. C. M., Neumann, R., dos Santos, I. D., & Dutra, A. J. B. (2020). Nickel and cobalt losses from laterite ore after the sulfation-roasting-leaching processing. *Journal of Materials Research and Technology, 9*(6), 12404–12415. https://doi.org/10.1016/j.jmrt.2020.08.082
38. Ribeiro, P. P. M., dos Santos, I. D., Neumann, R., Fernandes, A., & Dutra, A. J. B. (2021). Roasting and leaching behavior of nickel laterite ore. *Metallurgical and Materials Transactions B, 52*(3), 1739–1754. https://doi.org/10.1007/s11663-021-02141-6
39. Ribeiro, P. P. M., Neumann, R., dos Santos, I. D., & Dutra, A. J. B. (2022). An alternative route to extract nickel and cobalt from non-commercial laterite ore. *REM – International Engineering Journal, 75*(3), 245–257. https://doi.org/10.1590/0370-44672021750048

International Journal of Current Science Research and Review
ISSN: 2581-8341
Volume 09 Issue 07 July 2026
DOI: 10.47191/ijcsrr/V9-i7-59, Impact Factor: 8.048
IJCSRR @ 2026
www.ijcsrr.org

40. Sarı, Z. A., Turan, M. D., & Nizamoğlu, H. (2026). Thermal decomposition and leaching mechanisms of copper(II) oxalate (CuC_2O_4) raw material obtained from chalcopyrite concentrate. *Journal of Central South University*. Advance online publication. https://doi.org/10.1007/s11771-026-6353-8
41. ouza, R. F. M., Tavares, M. A. A., Cruz, L. E. C., Oliveira, V. A. A., Santos, I. D., Moura, F. J., & Brocchi, E. A. (2022). On the cobalt content upgrade in nickeliferous laterites using iron(III) sulfate: A study based on thermodynamics simulations. *Minerals, 12*(9), Article 1156. https://doi.org/10.3390/min12091156
42. Sun, Q., Cheng, H., Mei, X., Liu, Y., Li, G., Xu, Q., & Lu, X. (2020). Efficient synchronous extraction of nickel, copper, and cobalt from low-nickel matte by sulfation roasting–water leaching process. *Scientific Reports, 10*, Article 9916. https://doi.org/10.1038/s41598-020-66894-x
43. Sun, Y., Sun, G., Shi, Z., Yu, Q., & Wang, L. (2026). Thermodynamic modeling of selective sulfate roasting of copper–cobalt–iron sulfide ores: Phase transformation pathways and optimal process conditions. *Minerals, 16*(5), Article 497. https://doi.org/10.3390/min16050497
44. Taheri, B., & Larachi, F. (2025). Mineral-based magnesium extraction technologies: Current and future practices. *Processes, 13*(9), Article 2945. https://doi.org/10.3390/pr13092945
45. Tang, Y., Jia, X., Huang, C., Wang, F., Ren, Y., Gu, W., Li, R., Zhang, G., & Tang, M. (2023). Dissolution characteristics of typical iron-containing minerals. *Journal of Earth Environment, 14*(2), 136–144. https://doi.org/10.7515/JEE222007
46. Tauakelov, C. A., Rakhimbayev, B. S., Yskak, A., Valiev, K. K., Tastanov, Y. A., Ibrayev, M. K., Bulaev, A. G., Daribayeva, S. A., Kazbekova, K. A., & Joldassov, A. A. (2025). Treatment of refractory oxidized nickel ores (ONOs) from the Shevchenkovskoye ore deposit. *Metals, 15*(8), Article 876. https://doi.org/10.3390/met15080876
47. Teixeira, L. A. V. (2020). *Sulfation and selective roasting of rare earth elements in complex, iron-rich ores* [Doctoral thesis, Universidade Federal de Minas Gerais]. Repositório Institucional da Universidade Federal de Minas Gerais. https://hdl.handle.net/1843/39620
48. Thibault, Y., Gamage McEvoy, J., & Duguay, D. (2026). Key factors impacting the decomposition rate of REE silicates during sulfuric acid treatment. *Minerals, 16*(1), Article 31. https://doi.org/10.3390/min16010031
49. Thomas, M. (2021). Understanding gangue acid consumption in copper sulfide heap leaching: Predicting the impact of carbonates, silicates and secondary precipitates. *Minerals Engineering, 171*, Article 107090. https://doi.org/10.1016/j.mineng.2021.107090
50. Toro, N., Ghorbani, Y., Turan, M. D., Robles, P., & Gálvez, E. (2021). Gangues and clays minerals as rate-limiting factors in copper heap leaching: A review. *Metals, 11*(10), Article 1539. https://doi.org/10.3390/met11101539
51. Urtnasan, E., Kumar, A., & Wang, J.-P. (2024). Correlation between thermodynamic studies and experimental process for roasting cobalt-bearing pyrite. *Metals, 14*(7), Article 777. https://doi.org/10.3390/met14070777
52. Vehmaanperä, P., Salmimies, R., & Häkkinen, A. (2021). Thermodynamic and kinetic studies of dissolution of hematite in mixtures of oxalic and sulfuric acid. *Mining, Metallurgy & Exploration, 38*(1), 69–80. https://doi.org/10.1007/s42461-020-00308-4
53. Ventruti, G., Della Ventura, G., Gomez, M. A., Capitani, G., Sbroscia, M., & Sodo, A. (2020). High-temperature study of basic ferric sulfate, $FeOHSO_4$. *Physics and Chemistry of Minerals, 47*(10), Article 43. https://doi.org/10.1007/s00269-020-01113-7
54. Wan, X., Shi, J., Taskinen, P., & Jokilaakso, A. (2020). Extraction of copper from copper-bearing materials by sulfation roasting with SO_2–O_2 gas. *JOM, 72*(10), 3436–3446. https://doi.org/10.1007/s11837-020-04300-7
55. Wan, X., Taskinen, P., Shi, J., & Jokilaakso, A. (2021). A potential industrial waste–waste co-treatment process of utilizing waste SO_2 gas and residue heat to recover Co, Ni, and Cu from copper smelting slag. *Journal of Hazardous Materials, 414*, Article 125541. https://doi.org/10.1016/j.jhazmat.2021.125541
56. Wanderley, K. B., Botelho Junior, A. B., Espinosa, D. C. R., & Tenório, J. A. S. (2020). Kinetic and thermodynamic study of magnesium obtaining as sulfate monohydrate from nickel laterite leach waste by crystallization. *Journal of Cleaner Production, 272*, Article 122735. https://doi.org/10.1016/j.jclepro.2020.122735
57. Xiao, F., Liu, J., Yang, C., Shen, X., Yang, Z., Luo, X., Huang, H., Sun, S., & Tu, G. (2026). Sustainable valorization of limonitic laterite via phosphoric acid leaching: Selective recovery of nickel and cobalt with co-production of iron phosphate

under atmospheric conditions. *Journal of Cleaner Production, 561*, Article 148423. https://doi.org/10.1016/j.jclepro.2026.148423

58. Xiao, T., Mu, W., Shi, S., Xin, H., Xu, X., Cheng, H., Luo, S., & Zhai, Y. (2021). Simultaneous extraction of nickel, copper, and cobalt from low-grade nickel matte by oxidative sulfation roasting–water leaching process. *Minerals Engineering, 174*, Article 107254. https://doi.org/10.1016/j.mineng.2021.107254
59. Xu, Y.-J., Xin, H.-X., Duan, H.-M., Li, Y.-D., Wu, Y., Lin, J., & Zhai, Y.-C. (2022). Reaction behavior of silicon-rich diasporic bauxite with ammonium sulfate during roasting. *Journal of Central South University, 29*(1), 22–31. https://doi.org/10.1007/s11771-022-4917-9
60. Yang, X., Gao, L., Wu, Y., Chen, Y., & Tong, L. (2022). Extraction of magnesium and nickel from nickel-rich serpentine with sulfation roasting and water leaching. *Metals, 12*(2), Article 318. https://doi.org/10.3390/met12020318
61. Yeskibayeva, C., Auyeshov, A., Arynov, K., Dikanbayeva, A., & Satimbekova, A. (2024). Nature of serpentinite interactions with low-concentration sulfuric acid solutions. *Green Processing and Synthesis, 13*(1), Article 20240034. https://doi.org/10.1515/gps-2024-0034
62. Zhang, X., Wang, X., Guo, F., Hu, Y., Wu, J., Fan, W., Cui, J., Li, N., Zang, L., & Ma, R. (2026). Role of magnetite in high-temperature sulfuric acid roasting of Bayan Obo REE concentrate. *JOM*. Advance online publication. https://doi.org/10.1007/s11837-026-08192-x .
63. Zhao, Z., Li, H., & Wang, C. (2025). An integrated sulfation-roasting-leaching process for coextraction of nickel and cobalt from laterite ores with enhanced SO_3 recovery. *ACS Sustainable Resource Management, 2*(1), 201–211. https://doi.org/10.1021/acssusresmgt.4c00437.
64. Zhao, Z., Li, H., Wang, C., & Xing, P. (2025b). Selective and efficient extraction of nickel and cobalt from laterite ores using the sulfation-roasting and leaching-precipitation process with H_2O_2 and surfactant addition. *Hydrometallurgy, 237*, Article 106546. https://doi.org/10.1016/j.hydromet.2025.106546.
65. Zheng, G., Xia, J., Chen, Z., Yang, J., & Liu, C. (2020). Study on kinetics of the pyrolysis process of aluminum sulfate. *Phosphorus, Sulfur, and Silicon and the Related Elements, 195*(4), 285–292. https://doi.org/10.1080/10426507.2019.1686377.

Cite this Article: Pereira, A.C. (2026). Selective Iron Suppression through Sulfation, Oxidative Calcination, and pH-Controlled Atmospheric Leaching of a Ferruginous Oxidized Copper Ore. International Journal of Current Science Research and Review, 9(7), pp. 4155-4175. DOI: https://doi.org/10.47191/ijcsrr/V9-i7-59